Green synthesis of bentonite/cellulose@lead oxide bio-nanocomposite with assistance of *Pistacia Atlantica* extract for efficient photocatalytic degradation of ciprofloxacin

Atena Naeimi [a], Moones Honarmand [b],*, Mohammad Ali Chaji [b], Sepide Khosravi [a]

[a] *Department of Chemistry, Faculty of Science, University of Jiroft, Jiroft, Iran*
[b] *Department of Chemical Engineering, Birjand University of Technology, Birjand, Iran*

ARTICLE INFO

ABSTRACT

In this study, a novel bentonite/cellulose@lead oxide (BT-CL-PbO) bio-nanocomposite was synthesized *via* a green route. For this proposal, the extracted cellulose from barley waste and natural bentonite were bonded together by covalent bonding, and finally the biosynthesized lead oxide nanoparticles were immobilized on them. Then, due to the destructive impacts of antibiotic contaminants on the environment and ecosystem, the catalytic activity of nanocomposite was investigated for the photodegradation of ciprofloxacin. The BT-CL-PbO exhibited excellent catalytic activity over CIP degradation under sunlight. Effect of initial pH, ciprofloxacin concentration, BT-CL-PbO dosage, and the existence of anions on photocatalytic activity was studied. The photodegradation process of CIP fitted the pseudo-first-order kinetic model, and the rate constants in the presence of BT-CL-PbO reached 0.1309 min^{-1}, which was about 2.3 times higher than that of bare PbO nanoparticles. The scavenging experiments confirmed that photoexcited holes (h^+) played the prominent role in the photodegradation of CIP. The BT-CL-PbO showed high stability and reusability after three cycles of photodegradation. The obtained results found that the BT-CL-PbO is a cost-effective and recyclable photocatalyst for the photodegradation of CIP and can be used for the treatment of other pharmaceutical contaminants.

1. Introduction

Antibiotics are essential medicines to improve human and animal health, but in recent years, the pollution caused by them has become a global concern. Ciprofloxacin (CIP) is the third generation of fluoroquinolones antibiotic, which is used for the treatment of various diseases because of its broad-spectrum antibacterial activity [1,2]. CIP is found in wastewater of drug factories. Also, CIP released into the environment through human and animal feces due to its partial metabolism [3]. The presence of CIP in the environment causes the structure of microbial community to change over time, eventually leading to the emergence of bacteria with high drug resistance [4]. This is a severe threat to the ecosystem. Due to the destructive effects of CIP on the environment and ecosystem, the removal of these pharmaceutical contaminants has attracted the attention of scientists [5–10].

The conventional treatment methods are inefficient in removing contaminants in trace levels. Semiconductor-based photocatalysis has been known as an exciting solution for environmental problems [11–14]. Photodegradation is a simple, efficient and non-toxic, and cost-effective method for the removal of contaminants from wastewater. Different types of radicals that are produced using electrons and holes in the structure of photocatalyst are responsible for the degradation of pollutants. Lead oxide (PbO) nanoparticles (NPs) are a semiconductor that have broad applications in various fields due to their unique properties such as excellent photo conducting properties, extensive bandgap, and high thermal, chemical and mechanical stability [15]. The various physical and chemical methods were reported for the synthesis of PbO NPs [16–19]. However, the high energy and time are required in physical methods, and the production of toxic and environmentally harmful wastes in chemical routes has limited the synthesis of PbO NPs. To solve these shortcomings, biological processes were introduced for the green synthesis of nanoparticles

[20,21]. So far, limited studies have been done on the biosynthesis of PbO NPs using plant extracts [15,22–24].

Pistacia Atlantica is a fast-growing species that is found widely in Middle Eastern and Mediterranean regions. The fruits are edible and used in traditional and pharmaceutical medicine due to their antioxidant, antimicrobial, antipyretic, antiviral, and anti-inflammatory potential for treating various diseases [25,26]. Phytochemical studies on *Pistacia Atlantica* show that this plant contains many phenolic compounds [27,28]. The phenolic compounds are the principal agent of reduction of metal ions [29,30]. Thus, green synthesis of nanoparticles is well done using *Pistacia Atlantica*. In addition, the plant can be placed among the formed nanoparticles during the synthesis of nanoparticles, and to some extent prevents their agglomeration. Although extract in green methods and capping agents in chemical methods of nanoparticle synthesis is effective to avoid the agglomeration of nanoparticles, agglomeration is still observed. An excellent solution to this problem is to use different natural supports for the deposition of nanoparticles [31,32].

Bentonite (BT) is mineral clay, which is employed as cost-effective support for depositing catalysts/semiconductors due to large specific surface area, uniform pore volume, non-toxicity and, mechanical and thermal stability [33–35]. To enhance the interactions between support and active species, the BT surface can be modified with organic polymeric compounds. The organic compounds serve as a linker between support materials and nanoparticles, and act as an excellent platform for specific tasks. The O-H and C-H groups in the structure of organic compounds can establish strong interactions by hydrogen bonding, π-π heaping, and electrostatic interactions, thereby increasing the adsorption capacity of BT for the nanoparticles [36]. The organic compounds serve as a linker between support materials and nanoparticles, thereby increasing the adsorption capacity of BT for the nanoparticles.

Nowadays, a large amount of farming wastes was obtained by increasing efforts to production of agricultural which must be recycle. While, high energy consumption requires for their recycling. Some of developing countries were burned them leading to an important environmental pollution. On other hand, these materials are full of carbon and biomass to apply at various biofuels, biochemicals and biomaterials due to their different biological, chemical, and physical [37]. Indeed, they are very good candidate for production of biodegradable products and nanocomposites including lignocellulosic, and microorganisms. In fact, it seems that the changing the non-biodegradable materials with biodegradable nanocomposite with various properties is essential to diminish environmental pollutions [38–40]. According to reports and papers, wheat, barley and cotton have the highest amount of crop wastes [41,42]. Therefore, production of obtained nanocomposite from cellulose of crop wastes attract so much attention for real industrials applications, because cellulose is an effective-cost, biodegradable, available, non-toxic, and renewable raw biomaterial. They also can be modified through reactions of the active hydroxyl groups on the glucose units to have various applications.

Here, cellulose was extracted from barley wastes, and BT was provided from Birjand, Iran. Then, they were covalently attached through the formation of Schiff base ligand to obtain bentonite/cellulose. PbO NPs were synthesized using *Pistacia atlantica* extract. Finally, a novel bentonite/cellulose@ lead oxide bio-nanocomposite (BT- CL-PbO) was synthesized using biosynthesized PbO NPs and bentonite/cellulose. To our knowledge, the green synthesis of BT-CL-PbO bio-nanocomposite has not been reported in the literature. Then, to remove drug contamination, the synthesized BT-CL-PbO was utilized for the degradation of CIP under sunlight.

2. Experimental

2.1. Materials and methods

All chemicals were purchased from Merck and Aldrich Companies and used without further purification. Barley wastes and *Pistacia Atlantica* were collected from Jiroft and also bentonite from Birjand, Iran. Ciprofloxacin was supplied by Farabi pharmaceutical company (Iran). The crystal structure and composition of materials were studied by X-ray diffraction (XRD) on a Philips model PW 1800 X'pert diffractometer. The shape and particle size distribution of the BT-CL-PbO nanocomposite were specified by Transmission Electron Microscopy (TEM- ZEISS EM900) and High Resolution Transmission Electron Microscopy (HRTEM- Tecnai G2 F20 S-TWIN, FEI). Scanning electron microscopy and mapping analyses (TE-SCAN, MIRA3 FESEM model) were carried out to study the elemental composition and morphology of BT-CL-PbO nanocomposite. The concentration of CIP in the solutions after catalyst exposure was investigated by UV–Vis spectrophotometer (JENWAY-UK) at 273 nm with quartz cuvettes of 1 cm. The formed intermediates of CIP photodegradation were determined using an LC-MS analysis (Quattro Micro API micromass Waters 2695) that the column of the apparatus was Atlantis T3-C18 3μ, 2.1 × 100 mm. UV–Vis diffuse reflectance spectroscopy (DRS) of the synthesized nanocomposites was measured using a Shimadzu spectrophotometer (UV-2550 model). FT-IR spectra of the samples were recorded with a JASCO FT-IR 460 plus spectrophotometer in range of 400–4000 cm^{-1}.

2.2. Synthesis of amined bentonite

One gm of bentonite was added to 4 mL of (3-Aminopropyl) triethoxysilane in 30 mL ethanol and stirred at room temperature for 24 h. The aminated bentonite was separated using a centrifuge, and washed with ethanol and dried at 60 °C.

2.3. Synthesis of cellulose aldehyde

Sodium chlorite was added to *Barley wastes* at pH of value 3.8–4.0 and 75 °C to have brown holo-cellulose after filtering and washing with mixture water/ethanol for three times. The product was added to 10% KOH within 10 h and white micro cellulose was gained. Then, 4 g of extracted cellulose was dispersed in 80 mL distilled water under sonication. The stirring was continued at ambient temperature for 30 min. The above mixture was added into the 80 mL of distilled water and was oxidized with 5 g of sodium periodate (NaIO$_4$) in dark media. After three hours stirring at 55 °C, oxidation process was stopped *via* the adding an excess of ethylene glycol to reaction mixture. The obtained sample was filtered, washed several times with ethanol and distilled water and dried.

2.4. Synthesis of cellulose/bentonite composite

0.5 gm of cellulose aldehyde and 1 gm of aminated bentonite were mixed at 50 mL water with 5 min at 70 °C. After the condensation reaction between amine and aldehyde, the obtained cellulose/bentonite composite was washed with water and dried at 70 °C.

2.5. Synthesis of lead oxide NPs

4 gm of *Pistacia Atlantica* powder was added to 200 mL of boiled water and stirred for 15 min. After filtration, extracted *Pistacia Atlantica* solution was obtained. 70 mL of lead salt (0.1 M) and

70 mL water were added to 140 mL extracted *Pistacia Atlantica* solution at pH = 9 and stirred for two hours at 60 °C. Obtained participation was separated by centrifugation, and washed with water and dried at 60 °C. Then obtained green solid was heated at 489 °C for 90 min.

2.6. Synthesis of bentonite/cellulose@lead oxide (BT-CL-PbO) nanocomposite

1.5 gm of bentonite/cellulose in 20 mL water and 1 gm of lead oxide NPs in 20 mL of water were mixed and refluxed for five hours. Then, the result was washed with water and dried at room temperature.

2.7. Photodegradation tests

Batch experiments were performed in 100 mL Erlenmeyer flasks under sunlight on July 2021 in Birjand city (with radiation intensity of 260–280 Klux and where is located at latitude 32.8621 and longitude 59.193995) from 12p.m. to 2 p.m. with an average temperature of 33 °C. The BT-CL-PbO was dispersed into 50 mL of CIP aqueous solution and then stirred at darkness to achieve adsorption–desorption equilibrium for 30 min. Afterward, the mixed solution was exposed to sunlight. At regular intervals, about 3 mL of the suspension was taken out and separated by filter paper to remove the nanocomposites. The absorption spectrum of the filtrate was recorded using a UV–Vis spectrophotometer at 273 nm with quartz cuvettes of 1 cm. The degradation efficiency of CIP was calculated based on Eq. (1). C_0 and C_t (mg/L) are initial and final concentrations of CIP, respectively.

$$Degradation efficiency(\%) = \frac{C_0 - C_t}{C_0} \times 100 \qquad (1)$$

The effects of types of variables such as the initial pH value (3–9), the nanocomposite concentrations (0.2–2 g/L), and initial concentrations of CIP (10–100 mg/L) were evaluated under sunlight to obtain maximum degradation of CIP. HCl and NaOH (0.1 M) solutions were used to adjust the pH of the samples. Impacts of the common inorganic anions such as Cl^-, SO_4^{2-}, HCO_3^-, NO_3^-, and $H_2PO_4^-$ ions (prepared by dissolving 1 mmol of NaCl, Na_2SO_4, $NaHCO_3$, $NaNO_3$, and NaH_2PO_4 in 1 L water, respectively) were evaluated. The radical trapping experiments were performed using ammonium oxalate, 2-propanol, and benzoquinone as scavengers for h^+, $^•OH$, and $^•O_2^-$, respectively. The concentration of scavengers in the reaction mixture was 10 mmol/L. To evaluate the recyclability of the catalyst, at the end of each run, BT-CL-PbO was separated by centrifugation, washed several times with water, and dried for the next run.

3. Results and discussions

3.1. Characterization

The cellulose and bentonite were attached covalently using a condensation reaction between the aldehyde group of cellulose and the silanol and amine groups of bentonite to gain the bentonite/cellulose composite. Lead oxide NPs were synthesized using the *Pistacia Atlantica* plant under green media. Finally, mixing the lead oxide NPs and bentonite/cellulose composite led to fabricating BT-CL-PbO nanocomposite. This bio-nanocomposite was synthesized using natural and biodegradable starting materials without using any organic solvent.

The crystalline nature of the synthesized samples was determined using XRD. The XRD patterns of the BT, PbO NPs, and BT-CL-PbO were displayed in Fig. 1. In the XRD pattern of PbO NPs,

the diffraction peaks were observed at 2θ = 29.42° (1 0 1), 30.67°, 32.97°, 38.17°, 45.57° (2 0 0), 49.62° (2 0 1), 51.17°, 53.52° (2 1 1), 56.47°, 60.72° (1 0 3) and 63.42° (2 1 2). The related planes to several peaks of the corresponding PbO NPs were not marked with h k l values (refer JCPDS No. 01–0824) [43]. From the significant diffraction peak of the corresponding PbO (1 0 1) using the Debey–Scherrer equation, the particle size of PbO NPs was calculated 7 nm. After the immobilization of PbO NPs on bentonite/cellulose composite, not only was the crystalline structure of BT preserved, but also the peaks of PbO NPs are well seen in the diffraction pattern of BT-CL-PbO. The obtained results were confirmed the successful immobilization of PbO NPs on bentonite/cellulose composite.

The microstructure of the BT-CL-PbO nanocomposite was specified by TEM. As shown in Fig. 2a, PbO NPs (marked by the orange circle) with spherical morphology were observed in the TEM image of BT-CL-PbO. The HRTEM image of BT-CL-PbO showed that the biosynthesized PbO NPs were perfectly spherical with an average mean diameter of 7 nm and without any aggregation with each other (Fig. 2b). Moreover, the SAED patterns of BT-CL-PbO shown in Fig. 2c indicated the diffraction crystalline rings and white spots confirmed the high degree of crystalline and polycrystalline nature of biosynthesized BT-CL-PbO nanocomposite (Fig. 2c). The obtained "d" spacing equal to 0.309 nm was related to the (1 0 1) plane of tetragonal PbO NPs. These patterns exhibited that the well-crystallized PbO was fully consistent with the XRD results.

To obtain additional information of the BT-CL-PbO and dispersion quality of PbO NPs throughout composites, the BT-CL-PbO was characterized by SEM, EDS and elemental mapping images. The SEM images at different magnifications were demonstrated the spherical PbO NPs (marked by the orange circle) with less aggregation due to the efficient role of the biomolecules of extract as an excellent capping agent (Fig. 3a). Moreover, according to EDS spectrum, the weight percentage and the atomic percentage for carbon element were 44.59% and 66.13%, for oxygen element were 25.76% and 28.67%, for magnesium element were 0.91% and 0.67%, for aluminum element were 0.88% and 0.58%, for silicon element were 2.75% and 1.75%, for potassium element were 0.13% and 0.06% and for lead element were 24.97% and 2.15%, respectively (Fig. 3b). Besides, the elemental mapping images of BT-CL-PbO (Fig. 3c) illustrated which elements were uniformly distributed in the entire nanocomposite. The carbon element was related to cellulose, and the elements of magnesium, aluminum, silicon, and potassium were allocated to bentonite, and lead element was assigned to PbO NPs. The oxygen element was present in all three components of the composite. These results demonstrated that BT-CL-PbO was successfully prepared as designed.

The optical absorbance of BT-CL-PbO was measured by UV–Vis DRS. As shown in Fig. S1. BT-CL-PbO has good absorption capacity in the wide ultraviolet and visible region in the range of 200–600 nm. The bandgap energy of BT-CL-PbO was calculated by the Tauc plot of $(\alpha h\upsilon)^2$ vs. $h\upsilon$ [16] and determined to be 2.9 eV. According to this analysis, BT-CL-PbO could be an excellent photocatalyst for the efficient degradation of pollutants due to its wide absorption band [44].

The chemical structure of samples and interaction between cellulose aldehyde and amined bentonite were studied using FT-IR spectroscopy (Fig. 4). The FT-IR spectrum of the cellulose aldehyde contained bands of the stretching vibrations of the O-H groups at 3600–3000 cm^{-1}, C-H groups at 2880 cm^{-1} [45] and C = O groups at 1640 cm^{-1} [46]. A broad peak at 1371 cm^{-1} was attributed to the O-H bending vibrations and that at 1126 cm^{-1} was corresponded to the C-O antisymmetric bridge stretching [47]. The intense peak at 1060 cm^{-1} was related to C-O-C pyranose ring skeletal vibration [48]. In the FT-IR spectrum of amined bentonite,
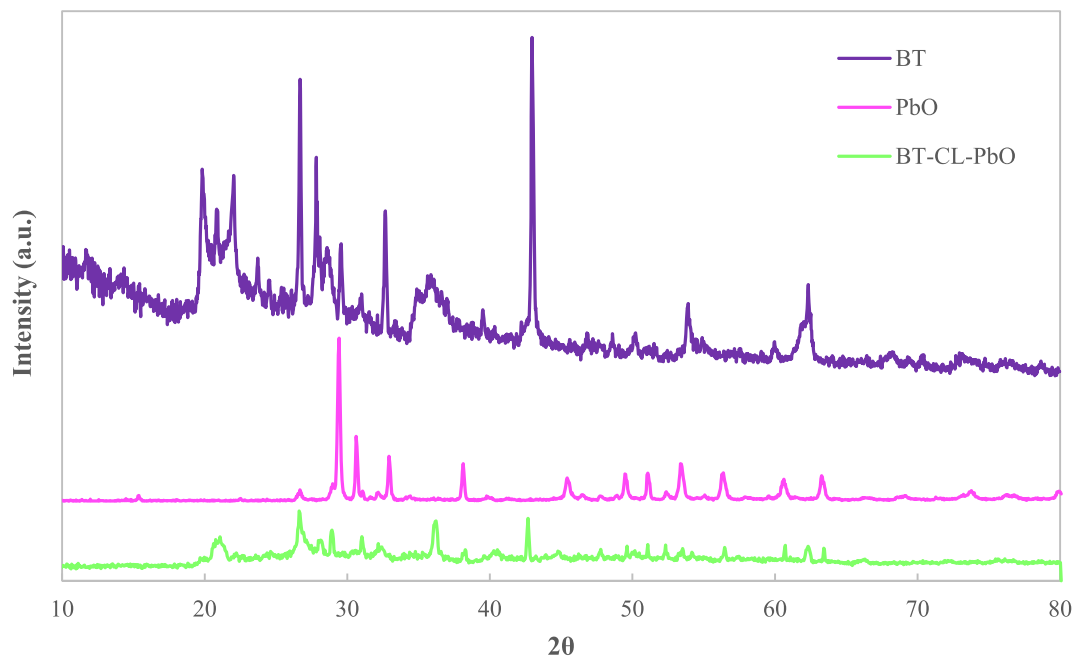
Fig. 1. The XRD pattern of BT, PbO NPs and BT-CL-PbO nanocomposites.
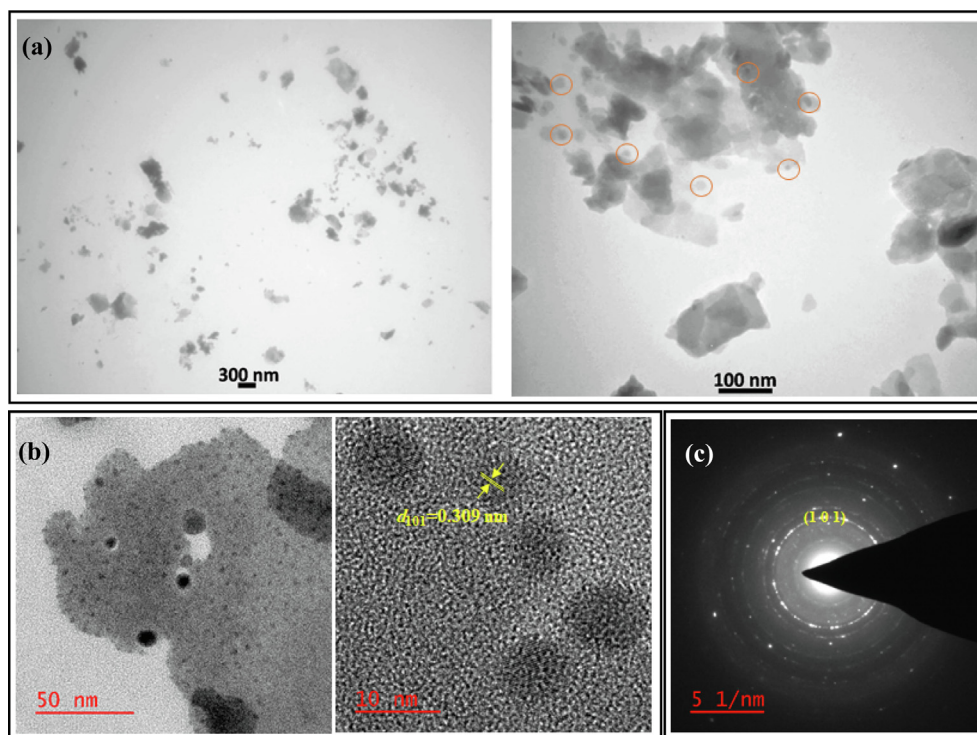

Fig. 2. (a) TEM, (b) HRTEM images (c) SAED patterns of BT-CL-PbO.

the broad bands in the range of 3650–3300 cm^{-1} were attributed to stretching vibrations of Si-OH groups of bentonite [49] and N-H groups of amined bentonite [36]. The appeared band at 1620 cm^{-1} was corresponded to the bending vibrations of the adsorbed water molecules. The strong band with the maximum at 1033 cm^{-1} was related to the Si-O-Si stretching vibrations in bentonite structure [50]. The two adsorption band at around 513 cm^{-1} and 420 cm^{-1} were ascribed to Si–O–Al and Si–O–Si

bending vibrations, respectively [51]. The FT-IR spectrum of the BT-CL-PbO displayed the considerable differences compared to the spectra of bare cellulose and bentonite. These differences were in the broadening and shorting of the absorption bands in the range of 3600–2850 cm^{-1}, 1500–1300 cm^{-1}, and 1640 cm^{-1}. Apparently, the collection of these changes in the spectrum of BT-CL-PbO was due to the formation of bonds between the oxygen-containing groups of the cellulose and the silanol and
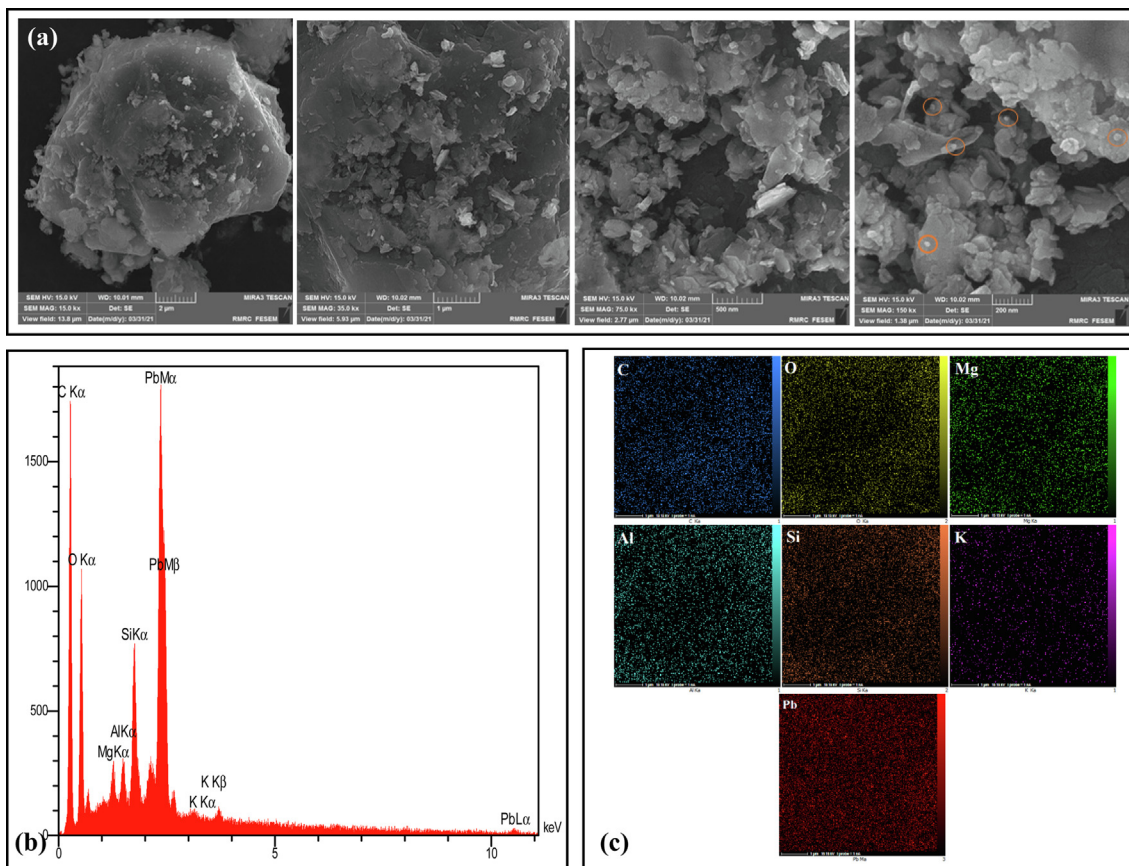
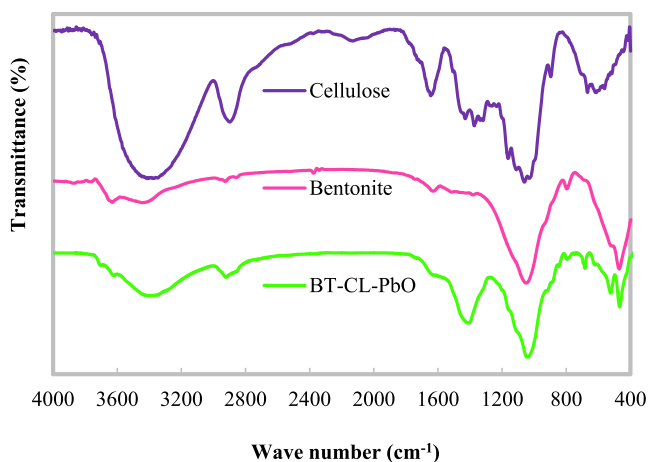**Fig. 3.** (a) SEM images, (b) EDS spectrum and (c) corresponding element mapping images of BT-CL-PbO.

Fig. 4. FT-IR spectra of cellulose, bentonite and BT-CL-PbO.

amine groups bentonite [52]. In the FT-IR spectrum of BT-CL-PbO two new peak appeared at 683 cm^{-1} and 524 cm^{-1}, which was assigned to the Pb–O bond [53].

3.2. Photodegradation of CIP

The photocatalytic degradation of CIP was investigated in the absence and presence of the different catalysts at neutral pH (6.3) under sunlight (Fig. 5). No degradation of CIP was seen in the absence of BT-CL-PbO even under sunlight after 30 min. The photocatalytic activity of the BT-CL-PbO was studied and compared with the bare PbO NPs. The degradation of CIP using

BT-CL-PbO and bare PbO NPs was 98.3% and 81.85%, respectively. The obtained results indicated that due to the synergetic effects of BT on PbO NPs, the presence of BT in structure of BT-CL-PbO is necessary for the boosting degradation efficiency of CIP. Also, the performance of bentonite and cellulose for the removal of CIP was investigated. The removal efficiency of CIP was obtained 26.91% and 15.13 % in the presence of bentonite and cellulose, respectively. For bentonite and cellulose, the removal efficiency of CIP mainly depended on their adsorption capacity for these two catalysts because the removal percentage in the presence of sunlight and the absence of sunlight was almost the same.

For better understanding the difference in the degradation activity, the rate constant was calculated as the equation for pseudo-first-order kinetic model:

$$-\ln\left(\frac{C}{C_0}\right) = k_{obs}t$$

where C_0 and C are the initial concentration and concentration of CIP (mg/L) at time t (min), respectively, and k_{obs} is the first-order rate constant (min^{-1}). The k_{obs} was calculated to be 0.1309, 0.0569, 00,104 and 0.0054 for BT-CL-PbO, PbO NPs, bentonite and cellulose, respectively. The obtained results showed that the removal of CIP using BT-CL-PbO was about 2.3, 12.5 and 23.9 times higher than bare PbO, bentonite and cellulose, respectively. The results showed that the combination of these three together leads to the emergence of an effective photocatalyst.

3.2.1. Effect of solution pH variation on the photodegradation efficiency

The effect of pH variation on the photocatalytic degradation of CIP using BT-CL-PbO was performed at pHs 3 to 9. As shown in
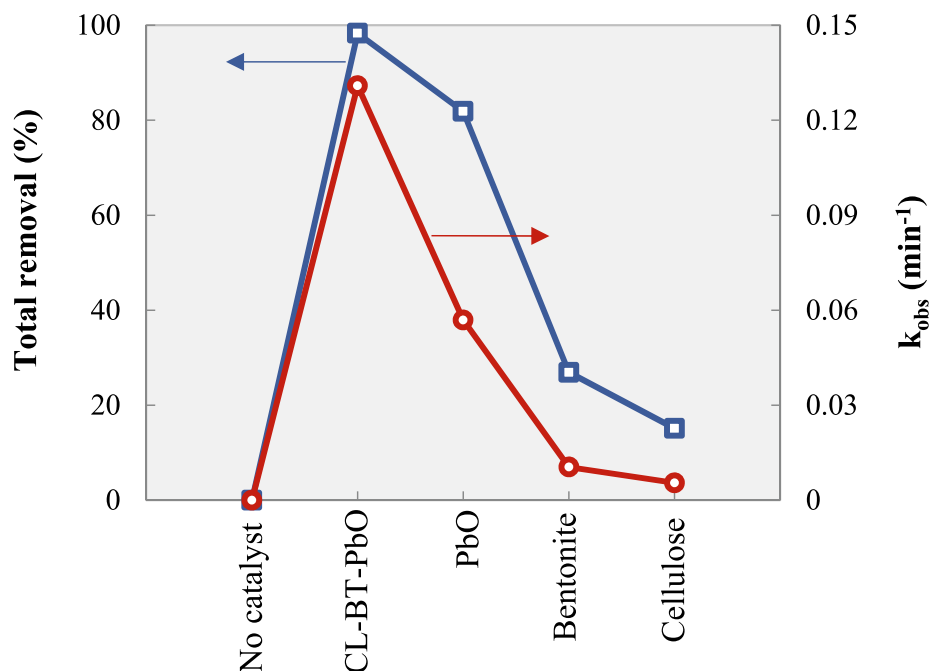
Fig. 5. Removal efficiencies of CIP and the corresponding k values in the presence of different catalysts.

Fig. 6a, the degradation efficiency of CIP was 50.29%, 58.06%, 82.82%, and 98.03% at pHs 3, 4, 5, and 6 respectively, after 30 min of irradiation. Following the pH increase, it was observed that with increasing the pH to 7, 8, and 9, the photodegradation of CIP decreased to 90.05%, 75.85%, and 64.48%, respectively. Based on these experiments, it was determined that pH = 6 was the best pH value, and the rest of the experiments were done at this pH. Furthermore, the adsorption of CIP onto BT-CL-PbO as a function of pH was tested in the darkness. The adsorption efficiency of CIP was in good agreement with the photodegradation patterns of CIP under sunlight at different pHs. The adsorption of CIP on BT-CL-PbO was 4%, 6%, 9%, 15%, 10%, 8% and 7% at pH 3, 4, 5, 6, 7, 8 and 9, respectively, after 30 min. The decrease in antibiotic adsorption on the catalyst surface under acidic and alkaline conditions was possibly due to repulsive forces between the positively and negatively charged BT-CL-PbO with the cationic and anionic CIP. The changes in photodegradation efficiency in various pHs could be attributed to the surface charges of CIP and BT-CL-PbO. As reported in the literature, pK_{a1} and pK_{a2} of CIP are 5.9 and 8.89, respectively, that means when pH is lower than 5.9, CIP is positively charged (CIP^+) because of the protonation of amine groups in the structure of CIP, while anionic form (CIP^-) exists when the pH is higher than 8.89 due to the deprotonation of carboxylic groups [11]. The zwitterionic CIP ($CIP^\pm$) exists when pH is in the range of 5.9–8.89. On the other hand, the point of zero charge (pH_{pzc}) of BT-CL-PbO was approximately obtained 5.6 (Fig. S2), which indicates charge BT-CL-PbO surface is positive at pH < 5.6, and then becomes negative at pH > 5.6. Under strongly acidic and alkaline conditions, the degradation of CIP is the least because of intense repulsion between the CIP molecules and BT-CL-PbO. However, the best degradation efficiency of CIP is at pH = 6 due to less repulsion between the CIP molecules and BT-CL-PbO. However, in the literature, there are reports in which the appropriate pH for the degradation of CIP is in the range of 5–7 due to the presence of a zwitterionic form of CIP and the more production of active radicals [54]. So, the optimum pH (6) in this study was consistent with the reported pH values.

For more emphasis, the k_{obs} for photodegradation of CIP in the presence of BT-CL-PbO was calculated using pseudo-first-order rate equation at various pHs. As displayed in Fig. 6b, the k_{obs} was increased from 0.0233 to 0.1309 when pH increased from 3 to 6. Then, the k_{obs} decreased to 0.0345 min^{-1} with further increasing pH to 9. As stated above, different species of CIP are strongly dependent on pH, and the k_{obs} for degradation of CIP can be expressed as:

$$k_{obs} = \sum \alpha_i k_i = \alpha_{CIP^-} k_{CIP^-} + \alpha_{CIP^\pm} k_{CIP^\pm} + \alpha_{CIP^+} k_{CIP^+}$$

$$\alpha_{CIP^+} = \frac{[H^+]^2}{[H^+]^2 + k_{a1}[H^+] + k_{a1}k_{a2}}$$

$$\alpha_{CIP^\pm} = \frac{k_{a1}[H^+]^2}{[H^+]^2 + k_{a1}[H^+] + k_{a1}k_{a2}}$$

$$\alpha_{CIP^\pm} = \frac{k_{a1}k_{a2}}{[H^+]^2 + k_{a1}[H^+] + k_{a1}k_{a2}}$$

where α_i is the molar fraction of CIP species, k_i is species-specific rate constant, and K_{a1} ($10^{-5.9}$) and K_{a2} ($10^{-8.89}$) are the dissociation constants of CIP. The $CIP^\pm$ is the predominant form with the highest k ($k_{CIP^\pm}$ = 0.108 min^{-1}), and then followed by CIP^- (k_{CIP^-} = 0.086 min^{-1}) and CIP^+ (k_{CIP^+} = 0.015 min^{-1}) [55].

3.2.2. Effect of initial concentration of CIP on the photodegradation efficiency

To study effect of the initial CIP concentration, the photodegradation of CIP was carried out at various CIP concentrations (from 10 to 100 mg/L) at pH = 6 (Fig. 6c). The results revealed that the degradation efficiency of CIP was decreased when the concentration of CIP increased. At higher concentrations (100 mg/L), this decrease is more dramatic. Some reasons have been suggested for this phenomenon: (1) the high concentration of CIP in the solution prevented sunlight from reaching to photocatalyst surface and reduced the formation of photogenic
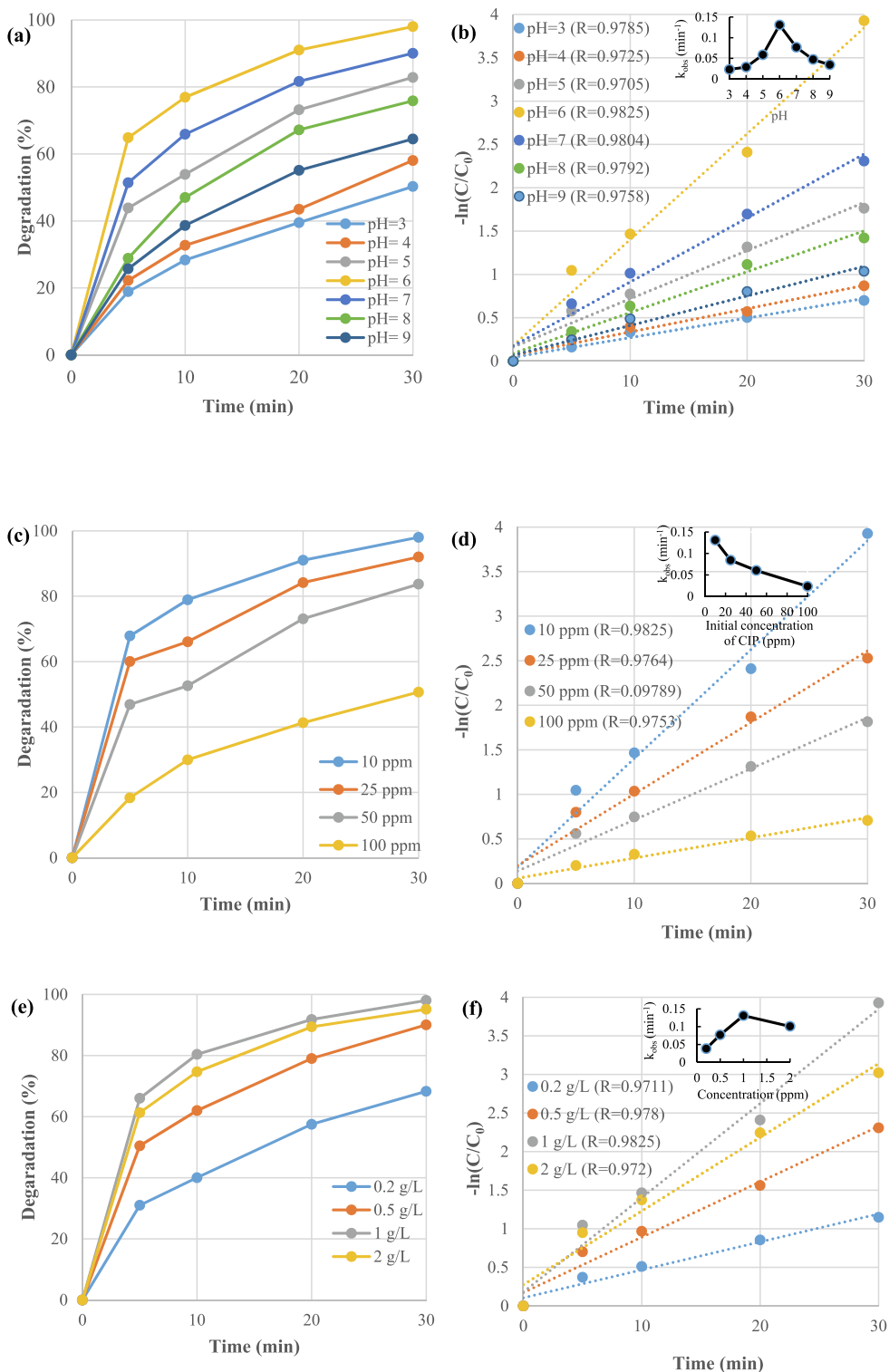
Fig. 6. Effect of (a) initial pH (c) CIP concentration (e) the dose of BT-LC-PbO nanocomposites on CIP degradation; kinetic of CIP degradation in various (b) pH (inset: k_{obs}), (d) CIP concentration (inset: k_{obs}), (f) the dose of BT-LC-PbO nanocomposites (inset: k_{obs}).

species, which in turn decreased the degradation efficiency. (2) At higher CIP concentrations, more intermediates were produced. These intermediates competed with CIP molecules for contact with active sites at the surface of BT-CL-PbO, which inhibited CIP photodegradation [56]. The reaction rate constant (k_{obs}) for

CIP photodegradation was illustrated in Fig. 6d and found to be 0.1309, 0.0849, 0.0604 and 0.0235 min^{-1} with 10, 25, 50 and 100 mg/L CIP, respectively. As the concentration of CIP was increased, the k_{obs} reduced and support the pseudo-first-order reaction.

3.2.3. Effect of the dosage of BT-CL-PbO on the photodegradation efficiency

To determine the optimal amount of BT-CL-PbO, the photodegradation efficiency of CIP was studied in the presence of various amounts of BT-CL-PbO. As shown in Fig. 6e, the photodegradation efficiency of CIP increased when the amount of BT-CL-PbO increased from 0.5 to 1.0 g/L. Conversely, the photodegradation yield decreased from 98.03 to 95.13% when the concentration of BT-CL-PbO increased from 1.0 to 2.0 g/ L. The k_{obs} values were 0.0383, 0.0769, 0.1309 and 0.1007 min^{-1} (R^2 > 0.97) when the amounts of BT-CL-PbO were 0.2, 0.5, 1 and 2 g/L, respectively (Fig. 6f). The low degradation efficiency at low photocatalyst amount was related to the limited active sites on the surface of BT-CL-PbO. The increase in dosage of BT-CL-PbO not only increases the number of actives sites for the adsorption of CIP molecules but also attract more sunlight to produce more active radicals. However, a further increase in the dosage of BT-CL-PbO (2 g/L) would lead to a reduction in the degradation performance of CIP because particles act as a mask on photosensitive surfaces, and the high turbidity of solution reduce the sunlight penetration and dispersion [55]. Therefore, the optimized dosage of BT-CL-PbO of 1.0 g/L was selected for further experiments.

3.2.4. Effect of inorganic anions on the photodegradation efficiency

Some inorganic anions such as chloride (Cl^-), sulfate (SO_4^{2-}), bicarbonate (HCO_3^-), nitrate (NO_3^-), and dihydrogen phosphate ($H_2PO_4^-$) are widely present in water and wastewater, which may interfere with the photodegradation of pollutants. So, effect of these ions on the degradation of CIP was investigated in the presence of BT-CL-PbO. The addition of anions (1 mM) to CIP solutions, reduced the performance of BT-CL-PbO, so that, the yield of CIP photodegradation was decreased from 98.03% in the absence of anions to 75.25–97.23% when anions were added. Also, the k_{obs} was reduced from 0.1309 min^{-1} in the absence of anions to 0.1195, 0.0988, 0.0624, 0.0594, and 0.0465 min^{-1} in the presence of Cl^-, NO_3^-, SO_4^{2-}, HCO_3^- and $H_2PO_4^-$ anions, respectively. The competition of these anions with CIP molecules for the active sites on the surface of BT-CL-PbO could be a reason for the reduction in the degradation performance of CIP. As shown in Fig. 7, the NO_3^- and
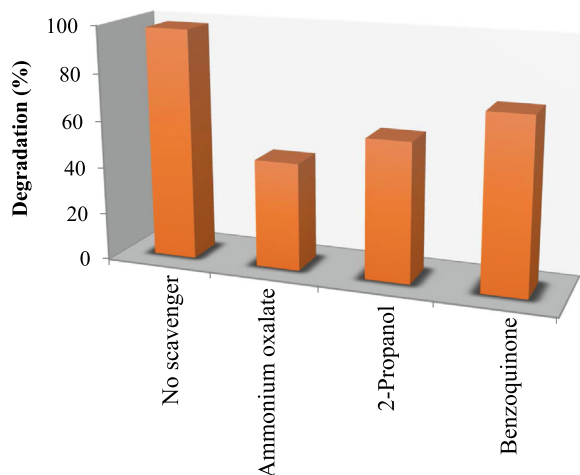

Fig. 8. Effect of scavengers on the CIP degradation in the presence of BT-CL-PbO.
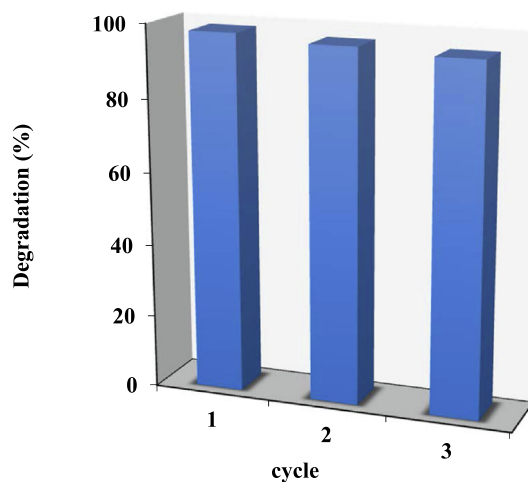

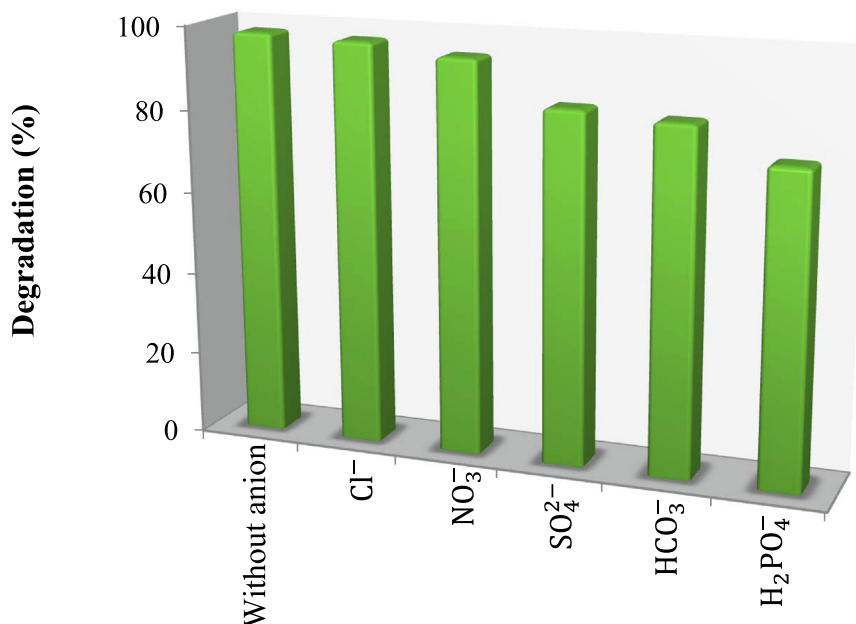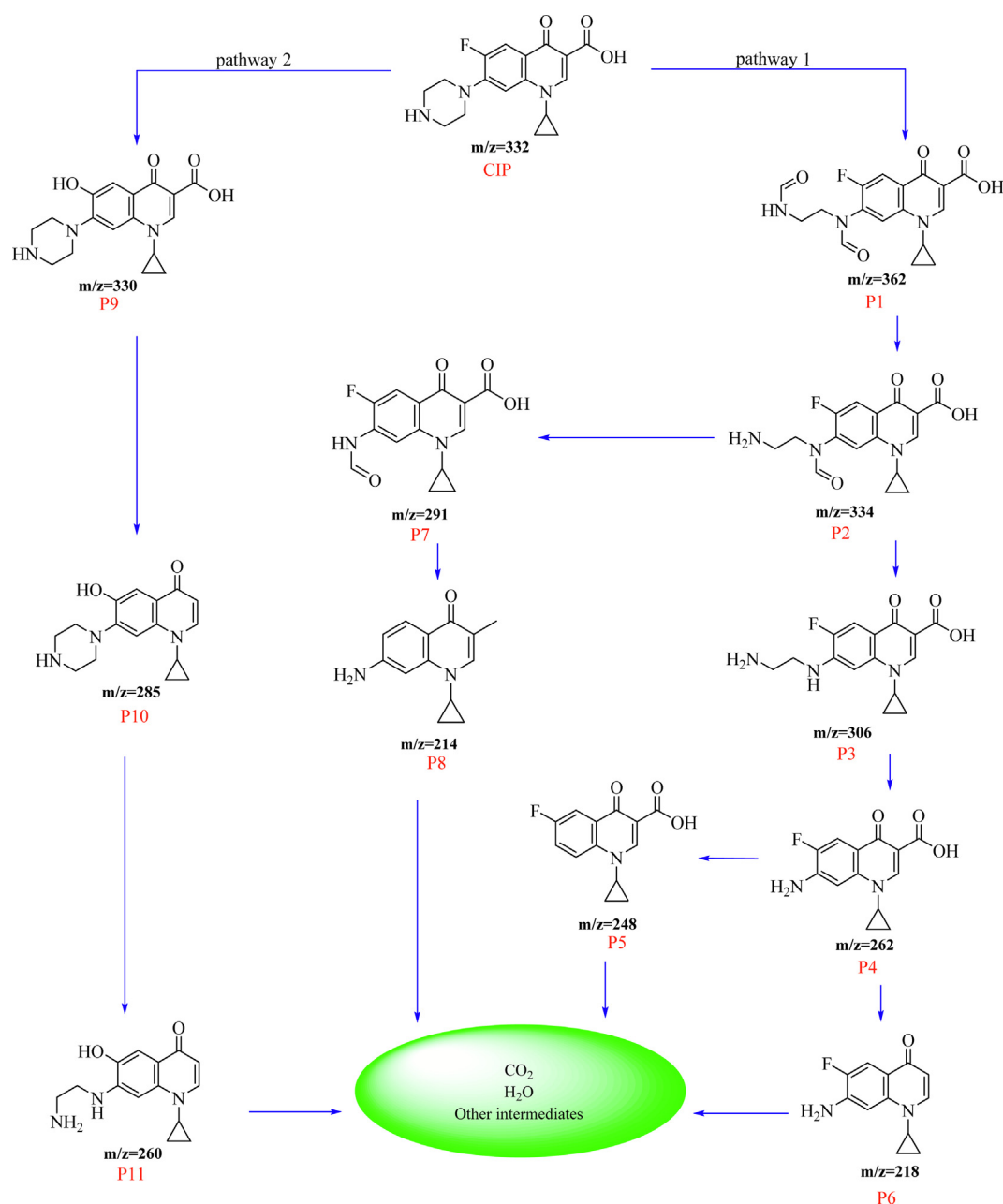**Fig. 9.** Recyclability test of the BT-CL-PbO in the degradation of CIP.

Fig. 7. Effect of ions on the CIP degradation in the presence of BT-CL-PbO.

Cl$^-$ ions have less inhibitory impact on the degradation of CIP than $H_2PO_4^-$, HCO_3^- andSO_4^{2-} anions.

The degradation of CIP was hampered in the presence of $H_2PO_4^-$ that was reacted with •OH and h$^+$ based on Eqs. (2) and (3). The produced H_2PO_4 radical is a weaker oxidizing agent than •OH radical [48,49], thus was seen the decreasing of the photodegradation of CIP. The SO_4^{2-} andHCO_3^- anions, according to Eqs. (4) and (5), were converted to SO_4^- and HCO_3^- radicals by reaction with the •OH radical [50,51]. HCO_3^- and SO_4^- radicals due to their large structure have higher selectivity than •OH radical, so it is less likely to react with CIP [57]. In the case of NO_3^- anion, the reduction of degradation efficiency of CIP was due to the N atom in piperazinyl structure of CIP molecule that was oxidized to NO_3^- by the attack of •OH radical, as stated in the Eq. (6). Given Le Chatelier's principle, the equilibrium was shifted to the left; as a result, photodegradation efficiency decreased [58]. According to Eqs. (7) and (8), the

Cl$^-$ was converted into HOCl$^{•-}$ radical that subsequently reproduced Cl$^•$ radical [59]. HOCl$^{•-}$ and Cl$^•$ radicals were both considerably influential towards the photodegradation of organic pollutants and maintained essentially the same •OH level, so the degradation performance was slightly decreased [60].

$$HPO_4^- + \cdot OH \rightarrow HPO_4 + -OH \tag{2}$$

$$HPO_4^- + h^+ \rightarrow HPO_4 \tag{3}$$

$$SO_4^{2-} + \cdot OH \rightarrow SO_4^- + H_2O \tag{4}$$

$$HCO_3^- + \cdot OH \rightarrow HCO_3^- + H_2O \tag{5}$$

$$(NR_3)_{CIP} + \cdot OH \rightarrow NO_3^- \tag{6}$$

$$Cl^- + \cdot OH \rightarrow HOCl^{•-} \tag{7}$$

Scheme 1. The proposed pathways of CIP photodegradation using BT-Cl-PbO under sunlight.

$$HOCl^- + H^+ \rightarrow Cl + H_2O \tag{8}$$

3.2.5. Effect of scavengers on the photodegradation efficiency

Effect of reactive oxygen species such as •OH and O_2^- radicals, and h^+ on the photocatalytic performance of BT- CL-PbO was investigated through the radical trapping experiments. As shown in Fig. 8, the degradation of CIP was decreased from 98.03% in the absence of scavengers to 45.78%, 59.04%, and 73.59% in the presence of ammonium oxalate, 2-propanol, and benzoquinone, respectively. Therefore, according to the obtained results, it can be concluded that although •OH and O_2^- radicals are responsible for part of the photocatalytic reaction, h^+ has the most significant role in the degradation of CIP.

3.2.6. Reusability and stability of BT-CL-PbO

Reusability is a considerable subject that is influencing the practical application of catalysts in environmental issues. The stability and reusability of BT-CL-PbO were studied by a three-cycle degradation of CIP. As displayed in Fig. 9, the catalytic performance of BT-CL-PbO was only slightly decreased after three cycles of photodegradation. The main reason for the high stability of the BT-CL-PbO was attributed to the strong bonding of PbO nanoparticles on bentonite.

3.2.7. Degradation pathways of CIP

The intermediates during the photocatalytic process of CIP were identified by LC–MS. Based on the comparative analysis of the LC-MS results with related literatures [10,46,56,57], two possible degradation pathways were proposed (Scheme 1). The LC-MS spectra of the produced intermediates during the CIP degradation process after 10, 20 and 30 min of irradiation were showed in Fig. S3. In pathway 1, the piperazine ring of CIP was attacked by the radicals and oxidized to produce amide P1 (m/z = 362) followed by losing the carbonyl group to form P2 (m/z = 334). In the following, P3 (m/z = 306) was produced after the elimination of another carbonyl group. Then, the piperazine moiety was completely separated from the CIP and produced P4 (m/z = 262). P5 and P6 were obtained through the decarboxylation and defluorination of P4, respectively. On the other hand, the radicals could be attacked to P2 and produced P7 (m/z = 291) by the removal of methylamine from P2. The decarboxylation and defluorination of P7 led to the formation of aniline P8 (m/z 214). Pathway 2 was started with a substitution reaction and P9 (m/z = 330) was produced by the replacement of fluorine group by hydroxyl group. The P9 was transformed into the P10 (m/z = 285) by the elimination of the carboxylic group and followed by breaking the piperazine ring and produced P11. As shown in Fig. S6, it could be seen that CIP was effectively degraded using BT-CL-PbO because the related peak of CIP (m/z = 333) was completely disappeared and lower mass intermediates were produced after 30 min.

4. Conclusion

In this study, bentonite/cellulose@lead oxide (BT-CL-PbO) bio-nanocomposite was synthesized as an efficient photocatalyst for degradation of ciprofloxacin. For the synthesis of BT-CL-PbO, the cellulose was extracted from barley wastes, natural bentonite was provided from mines of South Khorasan Province, and PbO nanoparticles were fabricated using *Pistacia Atlantica* plant. The crystalline nature, phase identification, morphology, size, and bandgap of BT-CL-PbO were analyzed by characterization techniques. Then, BT-CL-PbO was used as a green photocatalyst for the degradation of CIP under sunlight. Nearly complete degradation of CIP using BT-CL-PbO was observed within 30 min when initial pH, CIP concentration, and BT-CL-PbO dosage were 6, 10 ppm,

and 1 g/L, respectively. Effect of the existence of anions on the photocatalytic activity of BT-CL-PbO was studied, and the inhibitory effects on the CIP degradation were in the order of $H_2PO_4^- > HCO_3^- > SO_4^{2-} > NO_3^- > Cl^-$. The scavenger experiments indicated that h^+ has more contributor than other radicals in the degradation process. The results of reusability experiments demonstrated that BT-CL-PbO had good stability after three cycles of photodegradation. The results of this study show that BT-CL-PbO is an efficient and green photocatalyst that can open an avenue to fabricate semiconductors-based nanocomposites for practical applications in the purification of wastewater.

Declaration of Competing Interest

The authors declare that they have no known competing financial interests or personal relationships that could have appeared to influence the work reported in this paper.

Appendix A. Supplementary data

Supplementary data to this article can be found online at https://doi.org/10.1016/j.apt.2022.103441.

References

[1] N.T. Nguyen, T.H. Dao, T.T. Truong, T. Minh, T. Nguyen, T.D. Pham, Adsorption characteristic of cipro fl oxacin antibiotic onto synthesized alpha alumina nanoparticles with surface modi fi cation by polyanion, J. Mol. Liq. J. 309 (2020) 113150–113159.

[2] A. Raja, P. Rajasekaran, K. Selvakumar, M. Arunpandian, K. Kaviyarasu, S. Asath Bahadur, M. Swaminathan, Visible active reduced graphene oxide-BiVO₄-ZnO ternary photocatalyst for efficient removal of ciprofloxacin, Sep. Purif. Technol. 233 (2020) 115996–116004, https://doi.org/10.1016/j.seppur.2019.115996.

[3] S. Nekouei, F. Nekouei, H. Kargarzadeh, Synthesis of ZnO photocatalyst modified with activated carbon for a perfect degradation of ciprofloxacin and its secondary pollutants, Appl. Organomet. Chem. 32 (3) (2018) e4198, https://doi.org/10.1002/aoc.4198.

[4] F. Wang, X. Yu, M. Ge, S. Wu, One-step synthesis of TiO₂/γ-Fe₂O₃/GO nanocomposites for visible light-driven degradation of ciprofloxacin, Chem. Eng. J. 384 (2020) 123381–123389, https://doi.org/10.1016/j.cej.2019.123381.

[5] C. Li, N. Zhu, X. Dong, X. Zhang, T. Chen, S. Zheng, Z. Sun, Tuning and controlling photocatalytic performance of TiO₂/kaolinite composite towards ciprofloxacin: Role of 0D/2D structural assembly, Adv. Powder Technol. 31 (3) (2020) 1241–1252, https://doi.org/10.1016/j.apt.2020.01.007.

[6] Y.K. Manea, A.M. Khan, A.A. Wani, M.T.A. Qashqoosh, M. Shahadat, M.A.S. Salem, Hydrothermally synthesized mesoporous CS-g-PA@TSM functional nanocomposite for efficient photocatalytic degradation of Ciprofloxacin and treatment of metal ions, J. Mol. Liq. 335 (2021) 116144–116156, https://doi.org/10.1016/j.molliq.2021.116144.

[7] B. Zhu, D. Song, T. Jia, W. Sun, D. Wang, L. Wang, J. Guo, L. Jin, L.u. Zhang, H. Tao, Effective visible light-driven photocatalytic degradation of ciprofloxacin over flower-like Fe₃O₄–Bi₂WO₆ composites, ACS Omega 6 (2) (2021) 1647–1656, https://doi.org/10.1021/acsomega.0c0561610.1021/acsomega.0c05616.s001.

[8] K. Saravanakumar, C.M. Park, Rational design of a novel LaFeO₃/g-C₃N₄/BiFeO₃ double Z-scheme structure: Photocatalytic performance for antibiotic degradation and mechanistic insight, Chem. Eng. J. 423 (2021) 130076–130088, https://doi.org/10.1016/j.cej.2021.130076.

[9] V.S. Antonin, M.C. Santos, S. Garcia-Segura, E. Brillas, Electrochemical incineration of the antibiotic ciprofloxacin in sulfate medium and synthetic urine matrix, Water Res. 83 (2015) 31–41, https://doi.org/10.1016/j.watres.2015.05.066.

[10] J. Gao, D. Han, Y. Xu, Y. Liu, J. Shang, Persulfate activation by sulfide-modified nanoscale iron supported by biochar (S-nZVI/BC) for degradation of ciprofloxacin, Sep. Purif. Technol. 235 (2020) 116202–116209, https://doi.org/10.1016/j.seppur.2019.116202.

[11] A. Ulyankina, T. Molodtsova, M. Gorshenkov, I. Leontyev, D. Zhigunov, E. Konstantinova, T. Lastovina, J. Tolasz, J. Henych, N. Licciardello, G. Cuniberti, N. Smirnova, Photocatalytic degradation of ciprofloxacin in water at nano-ZnO prepared by pulse alternating current electrochemical synthesis, J. Water

Process Eng. 40 (2021) 101809–101818, https://doi.org/10.1016/j.jwpe.2020.101809.

[12] R. Gupta, B. Boruah, J.M. Modak, G. Madras, Kinetic study of Z-scheme C₃N₄/CuWO₄ photocatalyst towards solar light inactivation of mixed populated bacteria, J. Photochem. Photobiol. A Chem. 372 (2019) 108–121, https://doi.org/10.1016/j.jphotochem.2018.08.035.

[13] M. Golmohammadi, M. Honarmand, S. Ghanbari, A green approach to synthesis of ZnO nanoparticles using jujube fruit extract and their application in photocatalytic degradation of organic dyes, Spectrochim. Acta Part A Mol. Biomol. Spectrosc. 229 (2020) 117961–117969, https://doi.org/10.1016/j.jvb.2019.103347.

[14] M. Honarmand, M. Golmohammadi, A. Naeimi, Biosynthesis of tin oxide (SnO₂) nanoparticles using jujube fruit for photocatalytic degradation of organic dyes, Adv. Powder Technol. 30 (8) (2019) 1551–1557, https://doi.org/10.1016/j.apt.2019.04.033.

[15] S.K. Noukelag, H.E.A. Mohamed, L.C. Razanamahandry, S.K.O. Ntwampe, C.J. Arendse, Bio-inspired synthesis of PbO nanoparticles (NPs) via an aqueous extract of Rosmarinus officinalis (rosemary) leaves, Mater. Today Proc. 36 (2019) 421–426, https://doi.org/10.1016/j.matpr.2020.04.852.

[16] M. Nafees, M. Ikram, S. Ali, Thermal stability of lead sulfide and lead oxide nano-crystalline materials, Appl. Nanosci. 7 (7) (2017) 399–406, https://doi.org/10.1007/s13204-017-0578-7.

[17] S. Zeng, Y. Liang, H. Lu, L. Wang, X.-Q. Dinh, X. Yu, H.-P. Ho, X. Hu, K.-T. Yong, Synthesis of symmetrical hexagonal-shape PbO nanosheets using gold nanoparticles, Mater. Lett. 67 (1) (2012) 74–77, https://doi.org/10.1016/j.matlet.2011.09.048.

[18] B. Pathak, J. Prasad, R. Choudhury, P. Kumar, N. Aomoa, Optical properties of PbO/ZnO core/shell dispersed in PVP matrix, Mater. Today Proc. J. 46 (2021) 6196–6200, https://doi.org/10.1016/j.matpr.2020.04.158.

[19] R. Tayebee, B. Maleki, M. sabeti, A new simple method for the preparation of PbO nanoparticles and implementation of an efficient and reusable catalytic system for the synthesis of 1H-pyrazolo[1,2-b]phthalazine-5,10-diones, J. Iran. Chem. Soc. 14 (2017) 1179–1188, https://doi.org/10.1007/s13738-017-1068-2.

[20] Q. Sun, X. Cai, J. Li, M. Zheng, Z. Chen, C.P. Yu, Green synthesis of silver nanoparticles using tea leaf extract and evaluation of their stability and antibacterial activity, Colloids Surf. A Physicochem. Eng. Asp. 444 (2014) 226–231, https://doi.org/10.1016/j.colsurfa.2013.12.065.

[21] R. Shirmehenji, S. Javanshir, M. Honarmand, A green approach to the bio-based synthesis of selenium nanoparticles from mining waste, J. Clust. Sci. 32 (5) (2021) 1311–1323, https://doi.org/10.1007/s10876-020-01892-7.

[22] W. Muhammad, M.A. Khan, M. Nazir, A. Siddiquah, S. Mushtaq, S.S. Hashmi, B.H. Abbasi, Papaver somniferum L. mediated novel bioinspired lead oxide (PbO) and iron oxide (Fe₂O₃) nanoparticles: In-vitro biological applications, biocompatibility and their potential towards HepG2 cell line, Mater. Sci. Eng. C. 103 (2019) 109740–109750, https://doi.org/10.1016/j.msec.2019.109740.

[23] T. Sutjaritvorakul, S. Chutipaijit, Biological synthesis and characterization of lead oxide nanoparticles using Averrhoa bilimbi Linn. aqueous extract, AIP Conf. Proc. 2279 (2020) 130001–130006, https://doi.org/10.1063/5.0026158.

[24] E. Nazaripour, F. Mousazadeh, M. Doosti Moghadam, K. Najafi, F. Borhani, M. Sarani, M. Ghasemi, A. Rahdar, S. Iravani, M. Khatami, Biosynthesis of lead oxide and cerium oxide nanoparticles and their cytotoxic activities against colon cancer cell line, Inorg. Chem. Commun. 131 (2021) 108800–108808, https://doi.org/10.1016/j.inoche.2021.108800.

[25] N. Jomehzadeh, Z. Koolivand, E. Dahdouh, A. Akbari, A. Zahedi, N. Chamkouri, Investigating in-vitro antimicrobial activity, biosynthesis, and characterization of silver nanoparticles, zinc oxide nanoparticles, and silver-zinc oxide nanocomposites using Pistacia Atlantica Resin, Mater. Today Commun. 27 (2021) 102457–102466, https://doi.org/10.1016/j.mtcomm.2021.102457.

[26] M. Hamelian, S. Hemmati, K. Varmira, H. Veisi, Green synthesis, antibacterial, antioxidant and cytotoxic effect of gold nanoparticles using Pistacia Atlantica extract, J. Taiwan Inst. Chem. Eng. 93 (2018) 21–30, https://doi.org/10.1016/j.jtice.2018.07.018.

[27] A.A. Hatamnia, N. Abbaspour, R. Darvishzadeh, Antioxidant activity and phenolic profile of different parts of Bene (Pistacia atlantica subsp. kurdica) fruits, Food Chem. 145 (2014) 306–311, https://doi.org/10.1016/j.foodchem.2013.08.031.

[28] H. Veisi, M. Kavian, M. Hekmati, S. Hemmati, Biosynthesis of the silver nanoparticles on the graphene oxide's surface using Pistacia atlantica leaves extract and its antibacterial activity against some human pathogens, Polyhedron 161 (2019) 338–345, https://doi.org/10.1016/j.poly.2019.01.034.

[29] R. Golabiazar, K.I. Othman, K.M. Khalid, D.H. Maruf, S.M. Aulla, P.A. Yusif, Green synthesis, characterization, and investigation antibacterial activity of silver nanoparticles using pistacia atlantica leaf extract, Bionanoscience 9 (2) (2019) 323–333, https://doi.org/10.1007/s12668-019-0606-z.

[30] Z. Khiya, Y. Oualcadi, E.H. Mourid, I. Tagnaout, F. Berrekhis, T. Zair, F. El Hilali, Evaluation antioxidant and antibacterial activities of silver nanoparticles synthesized by aqueous extract of Pistacia atlantica, Res. Chem. Intermed. 47 (8) (2021) 3131–3144, https://doi.org/10.1007/s11164-021-04468-w.

[31] A. Soliemanzadeh, M. Fekri, The application of green tea extract to prepare bentonite-supported nanoscale zero-valent iron and its performance on removal of Cr(VI): Effect of relative parameters and soil experiments, Microporous Mesoporous Mater. 239 (2017) 60–69, https://doi.org/10.1016/j.micromeso.2016.09.050.

[32] M. Honarmand, M. Mirzadeh, M. Honarmand, Green synthesis of SnO₂-ZnO-eggshell nanocomposites and study of their application in removal of mercury

[33] (II) ions from aqueous solution, J. Environ. Heal. Sci. Eng. 18 (2) (2020) 1581–1593, https://doi.org/10.1007/s40201-020-00576-8.

[33] Q. Wang, B. Rhimi, H. Wang, C. Wang, Efficient photocatalytic degradation of gaseous toluene over F-doped TiO₂/exfoliated bentonite, Appl. Surf. Sci. 530 (2020) 1–12, https://doi.org/10.1016/j.apsusc.2020.147286.

[34] A. Rostami-Vartooni, M. Alizadeh, M. Bagherzadeh, Green synthesis, characterization and catalytic activity of natural bentonite-supported copper nanoparticles for the solvent-free synthesis of 1-substituted 1H-1,2,3,4-tetrazoles and reduction of 4-nitrophenol, Beilstein J. Nanotechnol. 6 (2015) 2300–2309, https://doi.org/10.3762/bjnano.6.236.

[35] M. Honarmand, M. Golmohammadi, A. Naeimi, Green synthesis of SnO₂-bentonite nanocomposites for the efficient photodegradation of methylene blue and eriochrome black-T, Mater. Chem. Phys. 241 (2020) 122416, https://doi.org/10.1016/j.matchemphys.2019.122416.

[36] Q.U. Ain, U. Rasheed, M. Yaseen, H. Zhang, Z. Tong, Superior dye degradation and adsorption capability of polydopamine modified Fe₃O₄-pillared bentonite composite, J. Hazard. Mater. 397 (2020) 122758–122775, https://doi.org/10.1016/j.jhazmat.2020.122758.

[37] R. Yevich, J.A. Logan, An assessment of biofuel use and burning of agricultural waste in the developing world, Global Biogeochem. Cycles. 17 (4) (2003) n/a–n/a, https://doi.org/10.1029/2002GB001952.

[38] K. Joshi, M.K. Meher, K.M. Poluri, Fabrication and characterization of bioblocks from agricultural waste using fungal mycelium for renewable and sustainable applications, ACS Appl. Bio Mater. 3 (4) (2020) 1884–1892, https://doi.org/10.1021/acsabm.9b01047.

[39] M.A. Martin-Luengo, M. Yates, M. Ramos, E. Saez Rojo, A.M. Martinez Serrano, L. Gonzalez Gil, E.R. Hitzky, Biomaterials from beer manufacture waste for bone growth scaffolds, Green Chem. Lett. Rev. 4 (3) (2011) 229–233, https://doi.org/10.1080/17518253.2010.544331.

[40] F.N. Al-Barakah, S.M. Radwan, R.A. Abdel-Aziz, Using biotechnology in recycling agricultural waste for sustainable agriculture and environmental protection, Int. J. Curr. Microbiol. Appl. Sci. 2 (2013) 446–459.

[41] R.R. Singhania, A.K. Patel, A. Pandey, 10 - Biotechnology for Agricultural Waste Recycling, in: 2017: pp. 223–240

[42] M. Prasad, R. Ranjan, A. Ali, D. Goyal, A. Yadav, T.B. Singh, P. Shrivastav, P.K. Dantu, Efficient transformation of agricultural waste in India, Contam. Agric. Sources, Impacts Manag. (2020) 271–287, https://doi.org/10.1007/978-3-030-41552-5_13.

[43] M. Salavati-Niasari, F. Mohandes, F. Davar, Preparation of PbO nanocrystals via decomposition of lead oxalate, Polyhedron 28 (11) (2009) 2263–2267, https://doi.org/10.1016/j.poly.2009.04.009.

[44] H.J. Das, A. Shah, L.R. Singh, M. Mahato, Waste derived low cost PbO-Carbon nanocomposite and its energy storage application, Mater. Today Proc. 47 (2021) 1072–1077, https://doi.org/10.1016/j.matpr.2021.06.434.

[45] V. Hospodarova, E. Singovszka, N. Stevulova, Characterization of cellulosic fibers by FTIR spectroscopy for their further implementation to building materials, Am. J. Anal. Chem. 09 (06) (2018) 303–310, https://doi.org/10.4236/ajac.2018.96023.

[46] Q.G. Fan, D.M. Lewis, K.N. Tapley, Characterization of cellulose aldehyde using Fourier transform infrared spectroscopy, J. Appl. Polym. Sci. 82 (5) (2001) 1195–1202, https://doi.org/10.1002/app.1953.

[47] J. Li, L.P. Zhang, F. Peng, J. Bian, T.Q. Yuan, F. Xu, R.C. Sun, Microwave-assisted solvent-free acetylation of cellulose with acetic anhydride in the presence of iodine as a catalyst, Molecules 14 (2009) 3551–3566, https://doi.org/10.3390/molecules14093551.

[48] W. Chen, H. He, H. Zhu, M. Cheng, Y. Li, S. Wang, Thermo-responsive cellulose-based material with switchable wettability for controllable oil/water separation, Polymers (Basel). 10 (2018) 592–617, https://doi.org/10.3390/polym10060592.

[49] K. Szostak, M. Banach, Sorption and photocatalytic degradation of methylene blue on bentonite-ZnO-CuO nanocomposite, J. Mol. Liq. 286 (2019) 110859–110874, https://doi.org/10.1016/j.molliq.2019.04.136.

[50] B. Krishnan, S. Mahalingam, Synthesis and characterization of Mn₃O₄/BC nanocomposite and its antimicrobial activity, J. Inorg. Organomet. Polym. Mater. 27 (1) (2017) 275–284, https://doi.org/10.1007/s10904-016-0470-z.

[51] B. Krishnan, S. Mahalingam, Ag/TiO₂/bentonite nanocomposite for biological applications: Synthesis, characterization, antibacterial and cytotoxic investigations, Adv. Powder Technol. 28 (9) (2017) 2265–2280, https://doi.org/10.1016/j.apt.2017.06.007.

[52] O.V. Alekseeva, A.N. Rodionova, N.A. Bagrovskaya, A.V. Agafonov, A.V. Noskov, Effect of the bentonite filler on structure and properties of composites based on hydroxyethyl cellulose, Arab. J. Chem. 12 (3) (2019) 398–404, https://doi.org/10.1016/j.arabjc.2015.07.011.

[53] M.E. Mahmoud, A.M. El-Khatib, M.S. Badawi, A.R. Rashad, R.M. El-Sharkawy, A.A. Thabet, Recycled high-density polyethylene plastics added with lead oxide nanoparticles as sustainable radiation shielding materials, J. Clean. Prod. 176 (2018) 276–287, https://doi.org/10.1016/j.jclepro.2017.12.100.

[54] B. Gupta, A.K. Gupta, C.S. Tiwary, P.S. Ghosal, A multivariate modeling and experimental realization of photocatalytic system of engineered S-C₃N₄/ZnO hybrid for ciprofloxacin removal: Influencing factors and degradation pathways, Environ. Res. 196 (2021) 110390–110402, https://doi.org/10.1016/j.envres.2020.110390.

[55] V.D. Dang, J. Adorna, T. Annadurai, T.A.N. Bui, H.L. Tran, L.Y. Lin, R.A. Doong, Indirect Z-scheme nitrogen-doped carbon dot decorated Bi₂MoO₆/g-C₃N₄ photocatalyst for enhanced visible-light-driven degradation of ciprofloxacin,

Chem. Eng. J. 422 (2021) 130103–130128, https://doi.org/10.1016/j.cej.2021.130103.

[56] X.J. Wen, C.G. Niu, L. Zhang, C. Liang, H. Guo, G.M. Zeng, Photocatalytic degradation of ciprofloxacin by a novel Z-scheme CeO_2–Ag/AgBr photocatalyst: Influencing factors, possible degradation pathways, and mechanism insight, J. Catal. 358 (2018) 141–154, https://doi.org/10.1016/j.jcat.2017.11.029.

[57] C. Zhao, Y. Li, H. Chu, X. Pan, L. Ling, P. Wang, H. Fu, C.C. Wang, Z. Wang, Construction of direct Z-scheme Bi_5O_7I/UiO-66-NH_2 heterojunction photocatalysts for enhanced degradation of ciprofloxacin: Mechanism insight, pathway analysis and toxicity evaluation, J. Hazard. Mater. 419 (2021) 126466–1124682, https://doi.org/10.1016/j.jhazmat.2021.126466.

[58] M. Chen, J. Yao, Y. Huang, H. Gong, W. Chu, Enhanced photocatalytic degradation of ciprofloxacin over Bi_2O_3/$(BiO)_2CO_3$ heterojunctions: Efficiency, kinetics, pathways, mechanisms and toxicity evaluation, Chem. Eng. J. 334 (2018) 453–461, https://doi.org/10.1016/j.cej.2017.10.064.

[59] C.-H. Liao, S.-F. Kang, F.-A. Wu, Hydroxyl radical scavenging role of chloride and bicarbonate ions in the H_2O_2/UV process, Chemosphere 44 (5) (2001) 1193–1200, https://doi.org/10.1016/S0045-6535(00)00278-2.

[60] M.J. Watts, K.G. Linden, Chlorine photolysis and subsequent OH radical production during UV treatment of chlorinated water, Water Res. 41 (13) (2007) 2871–2878, https://doi.org/10.1016/j.watres.2007.03.032.